THERMAL ANALYSIS OF END PUMPED FIBER LASERS SUBJECTED TO JACKET FLUID COOLING

Mamdouh EL HAJ ASSAD[1*], Ehab BANI HAN[2], Israa AL-SAWAFTA[1], Ahmad SEDAGHAT[2], M. ALSHABI[3], Shek RAHMAN[1]

[1] Sustainable and Renewable Energy Engineering Department, University of Sharjah, Sharjah, United Arab Emirates

[2] Mechanical Engineering Department, School of Engineering, Australian College of Kuwait, Kuwait

[3] Mechanical Engineering Department, University of Sharjah, Sharjah, United Arab Emirates

**Corresponding author*: massad@sharjah.ac.ae

End pumped lasers are highly efficient lasers particularly in diode lasers using micro lenses. The common cooling method for end-pumped systems is using water jacket or copper tube surrounding the laser rod. In this paper, the temperature distribution within a water jacket and a fiber laser end pumped by a top hat beam is studied analytically. The temperature distribution is obtained by considering the radial heat convection with fully developed laminar flow neglecting the axial heat conduction. The effect of laser dimensions and the Brinkman number on the temperature distribution are presented. The results indicate that the temperature distribution is strongly dependent on the Brinkman number. The results are presented in dimensionless form so that they can be applied to any end-pumped laser rod and fluid types. The main output of this work is that it is better for cooling purposes to have low Br values.

Key words: *Fiber laser, thermal distribution, Fluid coolant, Convection, Heat transfer*

Key words: *Laser rod, cooling, Temperature distribution*

1. Introduction

In general, laser devices are classified into four categories: solid state lasers, semiconductor, liquid (as dye lasers) and gaseous. They are mainly composed of optical resonator, pumping source and an active medium. The active medium of solid state lasers is made of crystal or glass. An external optical source provides energy to the optical resonator where the active medium is placed inside. Laser is a monochromatic and intense light beam that is produced by stimulated emission of radiation of a light source [1]. Laser pumping is then referred as the energy transfer to the active medium from the external source.

Diode lasers are widely used and has many medical and industrial applications from metal cutting to oral surgery [1-3]. Potentially diode lasers are considered as the cheapest laser technology, as long as the requirements of the manufacturing process of diode laser are met. Other advantages that motivate the use of these lasers are their efficiency, maintenance requirements or compactness. In addition, the possibility of a process specific tailored polarization or wavelength can be an option to consider. Recent studies have indicated a great potential of polarization control with diode lasers in laser cutting [4]. Diode lasers are known as high power sources and they have the ability to produce beam quality [5, 6]. In these types of lasers, the pumping process occurs through two methods namely the Continuous Wave (CW) and Pulse Pumping (PP) laser systems. Besides, Diode Pumped Solid State (DPSS) lasers are categorized into Side Pumped (SP) and End Pumped (EP) configurations [7]. Figure 1 presents a schematic of solid state typical lasers with the aforementioned pumping configurations.

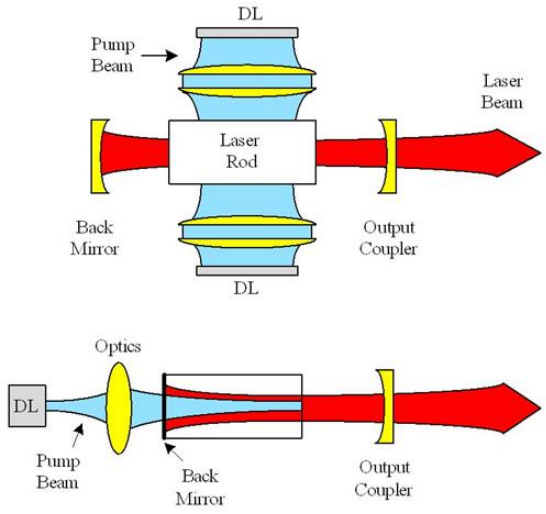

Figure 1. Pumping methods of the gain medium of solid state laser: side pumping (top) and end pumping (bottom) [7]

Lasers can be made in different forms such as bulk, fiber, disk, and Microchip lasers [8-15]. The heat generation is associated with optical pumping in solid state laser materials in which the temperature profile of a continuous-wave end-pumped solid-state laser with a solid heat sink at the periphery [16] . Transferring heat to the surrounding medium for cooling which is spatial and time dependent causes thermal gradient inside the gain medium [17] where uniform power heat power deposition into the fiber was considered. The heat transfer flows from the center of the laser rod toward the laser rod outer surface which is exposed to cooling. For instance, the main portion of heat removal takes place through the radial direction in fiber lasers and traditional rod shape laser mediums with water cooling configuration, this leads to a considerable radial thermal gradient in the inner side of the medium as shown in Figure 2.

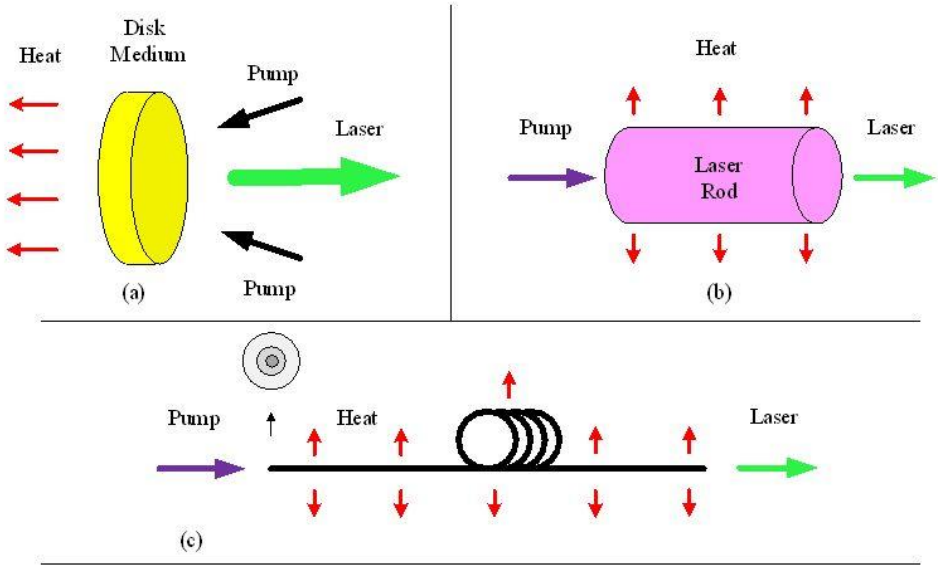

Figure 2. A schematic of heat transfer direction in fiber laser type of solid state lasers [7]

This is the responsible reason for the undesirable appearance of thermal effects on the operation of lasers. There are some detrimental effects like thermal lensing [18], thermal stress fracture limit [19], thermal birefringence and thus thermal bi-focusing [20-23] that should be reduced to minimal. Temperature distribution must be determined within the fiber laser and the gain medium in order to optimize the performance of fiber laser. This is dependent on the beam intensity profile of pump laser, thermal properties (crystalline rod or glass fiber), cooling medium and geometry.

The heat differential equation should be solved together with proper boundary conditions to give the temperature field. The boundary conditions depend on the cooling methods whether conductive or convective heat transfer to the surrounding medium. Water cooling is the most common method used in the operations of high power lasers. Determining the temperature distribution inside the laser rod and cooling medium has an important role in the evaluation of induced thermo-optic effects on laser operation.

Nd:YAG laser rods has been under lot of research by applying Gaussian distribution for thermal analysis of end-pumped pumping and cooling with constant temperature at the surface of the laser rod [18]. Other studies have considered the thermal behavior of laser crystal rods using semi analytical analysis [19, 20]. Convective cooling techniques have been applied at the boundary of long fiber laser [21], [22]and short fiber lasers [23]. In general, radiation heat transfer is neglected in the thermal analysis of laser rods [17-24]. End pumping effect result in non-uniform heat generation within the laser rod which leads to non-uniform and complicated energy equation. Hence, numerical technique has been applied to simulate laser medium thermal problem in order to solve the high non-linearity of heat equation [25, 26]. Two dimensional solution of the temperature has been solved analytically in the fiber laser and cladding considering top-hat beam [27] where the results can be applied for the same thermal conductivity of the fiber and cladding. The prediction of steady state temperature distribution in Nd:YAG laser rod has been obtained using finite element analysis [28] where the laser rod was cooled by water. Transient temperature distribution in CW-End-pumped laser rod has been obtained analytically [29] where thermal stress distribution has been also obtained. Another analytical work derived the transient temperature distribution in pulsed solid-state laser rod [30]. The results of this study give options to designers to select the pulse width, period and cycle duty in order to prevent the fracture in laser rod. In other work [31], a detailed analytical solution of laser rod with large aspect ratio has been carried out to find the temperature distribution within the laser rod when it is surrounded by cladding as a heat sink. One way to optimize the performance of any thermal system can be done by applying second law of thermodynamics in terms of entropy generation. Laser surface treatment for a fiber laminated plate with coating layer has been investigated using three-dimensional transient thermodynamic analysis [32]. Fiber orientation for a laminated plate has a great influence on the deflection, normal stress and shear stress of the piezoelectric laminated plate [33]. Steady state thermodynamic analysis of double layer using three dimensional heat conduction theory and laminated plate theory has been conducted to find out the parameters that effect the behavior of the double layer [34] The analysis of entropy generation has been proved to be an efficient method to optimize the performance of heat exchange process in heat exchangers [35], slabs with non-uniform internal heat generation [36, 37] and fiber laser rod [31]. This paper presents a thermal analysis model of a fiber laser with an aim to determine the temperature distribution inside the laser rod subjected to a convective cooling at its surface. The model is only valid for laminar fluid flow and the results are applicable to fiber lasers or crystalline rod that contain an active core and surrounding coolant.

2. Mathematical formulations

Energy equation for laser rod and fluid flow can be expressed as, respectively

$$\frac{1}{r}\frac{\partial}{\partial r}\left(r\frac{\partial T}{\partial r}\right)+\frac{\partial^2 T}{\partial z^2}+\frac{q_v(r,z)}{k}=0 \tag{1}$$

$$u\frac{\partial T}{\partial z}=\frac{k}{\rho c_p}\frac{1}{r}\frac{\partial}{\partial r}\left(r\frac{\partial T}{\partial r}\right)+\frac{\mu}{\rho c_p}\left(\frac{du}{dz}\right)^2 \tag{2}$$

where T is the temperature, u is the velocity, ρ is the density, μ is the dynamic viscosity, k is the thermal conductivity, c_p is the specific heat, r is the radial direction and z is the axial direction. The volumetric heat generation within the laser rod is expressed as

$$q_v=\frac{\alpha\xi P_o e^{-\alpha z}}{\pi r_i^2(1-e^{-\alpha L})} \tag{3}$$

where α is the absorption coefficient, ξ is the thermal factor, P_o is the pumping power and L is the laser rod length.

Equation (3) is valid only within the laser rod for $r \le r_i$ and it is equal to zero within the fluid for $r_i < r \le r_o$

The velocity distribution of the fluid flow around the laser rods is expressed as

$$U=\frac{u}{u_m}=-2\frac{\left[r^2-r_i^2+\left(r_o^2-r_i^2\right)\dfrac{\ln\left(\frac{r_i}{r}\right)}{\ln\left(\frac{r_o}{r_i}\right)}\right]}{r_o^2+r_i^2-\dfrac{r_o^2-r_i^2}{\ln\left(\frac{r_o}{r_i}\right)}} \tag{4}$$

where the mean velocity of fluid is $u_m=\frac{2}{\left(r_o^2-r_i^2\right)}\int_{r_i}^{r_o} u\,r\,dr$, r_i and r_o are the inner and outer radius, respectively.

Defining the following non-dimensional parameters as $r^*=\frac{r}{r_o}$, $a^*=\frac{r_i}{r_o}$, $A_r=\frac{L}{2r_o}$, $\alpha_L=\alpha L$, $z^*=\frac{z}{L}$, and $\theta=4\pi kL\frac{T-T_W}{Q}$, the laser rod temperature given in Eq. (1) can be obtained as

$$\frac{1}{r^*}\frac{d}{dr^*}\left(r^*\frac{d\theta}{dr^*}\right)+\frac{1}{A_r^2}\frac{d^2\theta}{dz^{*2}}+4\pi Lr_o^2F(r^*,z^*)=0 \tag{5a}$$

where $F(r^*,z^*)=\frac{ae^{-\propto_L z^*}}{\pi a^{*2}r_o^2(1-e^{-\propto_L})}$.

Neglecting the second term of Eq. (5a) due to high aspect ratio A_r, Eq. (5a) can be written as

$$\frac{1}{r^*}\frac{d}{dr^*}\left(r^*\frac{d\theta}{dr^*}\right)+\frac{4\alpha_L e^{-\propto_L z^*}}{a^{*2}(1-e^{-\propto_L})}=0 \tag{5b}$$

Eq. (5b) can now be integrated twice with respect to give the following temperature distribution in the

laser rod as

$$\theta_{rod}(r^*, z^*) = -\frac{A}{4} r^{*2} e^{-\alpha_L z^*} + C_1 \ln(r^*) + C_2 = 0 \quad (5c)$$

where $A = \frac{4\alpha_L}{a^{*2}(1-e^{-\alpha_L})}$, C_1 and C_2 are integration constants, T_w is the outer surface temperature of the fluid and $Q = \int_V q_v(r,z)dV = \xi P_o$.

It is interesting that Eq. (5c) gives the rod distribution as function of r and z directions though the aspect ratio is high ($\frac{1}{A_r}\frac{\partial^2 T}{\partial z^2} \to 0$). This is due to the fact the internal heat generation is function of z.The energy equation of fluid flow is expressed in dimensionless form as

$$\frac{1}{r^*}\frac{\partial}{\partial r^*}\left(r^* \frac{\partial \theta_f}{\partial r^*}\right) = -\frac{4\pi kL}{Q}\frac{u_m^2 P_r}{C_p}\left(\frac{dU}{dr^*}\right)^2 \quad (6)$$

Defining Brinkman number as $B_r = \frac{\mu u_m^2}{(\frac{Q}{2\pi r_i L})r_i}$, Equation 2 can be written as

$$\frac{1}{r^*}\frac{\partial}{\partial r^*}\left(r^* \frac{\partial \theta_f}{\partial r^*}\right) = -2\frac{k}{k_f} B_r r^* \frac{4}{(1+a^{*2}+\frac{1-a^{*2}}{lna^*})^2}\left[2r^* + \frac{1-a^{*2}}{r^* lna^*}\right]^2 \quad (7)$$

Let $M = -2\frac{k}{k_f} B_r \frac{4}{(1+a^{*2}+\frac{1-a^{*2}}{lna^*})^2}$ and $N = \frac{1-a^{*2}}{lna^*}$ then Eq. (7) is written as:

$$\frac{d}{dr^*}\left(r^* \frac{d\theta_f}{dr^*}\right) = Mr^*(2r^* + \frac{N}{r^*})^2 \quad (8)$$

Integrating twice Eq. (8) gives

$$\theta_f = \frac{1}{4} Mr^{*4} + MNr^{*2} + \frac{1}{2} MN^2 (\ln(r^*))^2 + \mathrm{D}\ln(r^*) + E \quad (9)$$

where D and E are integration constants.

In Eq (9) derivation, high aspect ratio A_r is still considered, that is why $\frac{1}{A}\frac{\partial T}{\partial z} \to 0$ but the fluid temperature is function of r and z when the boundary conditions are written.

The boundary conditions that taking into account the fluid is flowing at very small velocity used in the analysis, are

$$T_{rod}(r=0) = finite \to \theta_{rod}(r^*=0) = finite \quad (10)$$

$$T_{rod}(r=r_i) = T_f(r=r_i) \to \theta_{rod}(r^*=a^*) = \theta_f(r^*=a^*) \quad (11)$$

$$k\frac{dT_{rod}}{dr}\Big|_{r=r_i} = k_f \frac{dT_f}{dr}\Big|_{r=r_i} \Rightarrow k\frac{d\theta_{rod}}{dr^*}\Big|_{r^*=a^*} = k_f \frac{d\theta_f}{dr^*}\Big|_{r^*=a^*} \quad (12)$$

$$T_f\Big|_{r=r_0} = T_w(wall\ temperature) \Rightarrow \theta_f\Big|_{r^*=1} = 0 \quad (13)$$

Applying the above four boundary conditions to find out the integral constants of the laser and fluid temperatures in Equations (5) and (9), respectively as

$$C_1 = 0 \text{ and } C_2 = \frac{A}{4}a^{*2}e^{-\alpha_L z^*} + \frac{1}{4}Ma^{*4} + MNa^{*2} + \frac{1}{2}MN(\ln(a^*))^2 + Dlna^* + E$$

where $E = -MN - \frac{1}{4}M$, $D = -\frac{A}{2}a^{*2}e^{-\alpha_L z^*}\frac{k}{k_f} - Ma^{*2} - 2MNa^{*2} - MN\ln a^*$

Using $C_1, C_2, D, and\ E$, the rod and fluid temperatures are obtained as, respectively

$$\theta_{rod} = \frac{\alpha_L}{1-e^{-\alpha_L}}e^{-\alpha_L z^*}\left[1 - \left(\frac{r^*}{a^*}\right)^2 - 2\frac{k}{k_f}lna^*\right] + Ma^{*2}\left[\frac{a^*}{4} + N - 2Nlna^* - a^{*2}lna^*\right] -$$

$$\frac{1}{2}MN^2(lna^*)^2 - M(\frac{1}{4} + N) \qquad (14)$$

$$\theta_f = \frac{1}{4}Mr^{*4} + MNr^{*2} + lnr^*\left[\frac{1}{2}MN^2lnr^* - \frac{2\alpha_L}{1-e^{-\alpha_L}}\frac{k}{k_f}e^{-\alpha_L z^*} - Ma^{*4} - 2MNa^{*2} - MN^2lna^*\right] -$$

$$M(\frac{1}{4} + N) \qquad (15)$$

where k_f is the fluid thermal conductivity and $a^* = \frac{r_i}{r_o}$.

Equations (14) and (15) are both function of $r^*$and z^* even though high aspect ratio is considered.

3. Results and Discussion

The temperature distributions of laser rod and fluid are obtained in this section by using some numerical values for $\frac{k}{k_f} = 0.2$.

Figures 3-5 outline the dimensionless temperature distribution in the laser rod including the fluid as function of the dimensionless axial direction at different r* locations for Br=0.001, 0.1 and 1, respectively. The figures show that increasing Br number results in higher temperature for the same r* value. This is due to the fact that high Br number physically means that the heat produced by viscous dissipation is conducted slowly. The temperature increases as r* decreases because the heat generation of the laser rod is maximum at the centerline of the rod (r*=0). Figure 3-5 also show that the temperature decreases in axial direct but the decrease is slower at higher r* values (i.e. r*=0.8) because as we approach r*=1 (outer surface of fluid), the temperature remains constant (equal to wall temperature) as mentioned in the boundary conditions.

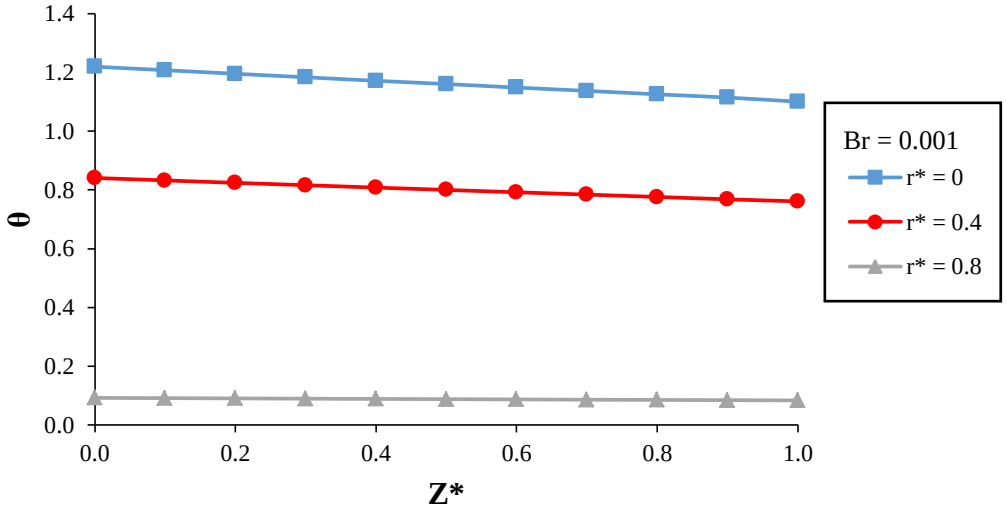

Figure 3: Laser rod temperature as a function of dimensionless length at different dimensionless radius for Br = 0.001

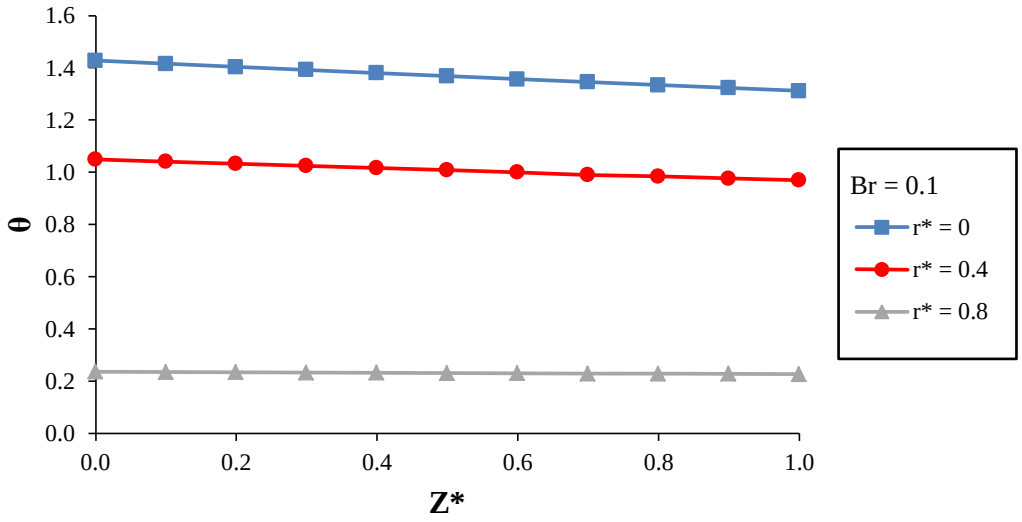

Figure 4: Laser rod temperature as a function of dimensionless length at different dimensionless radius for Br = 0.1

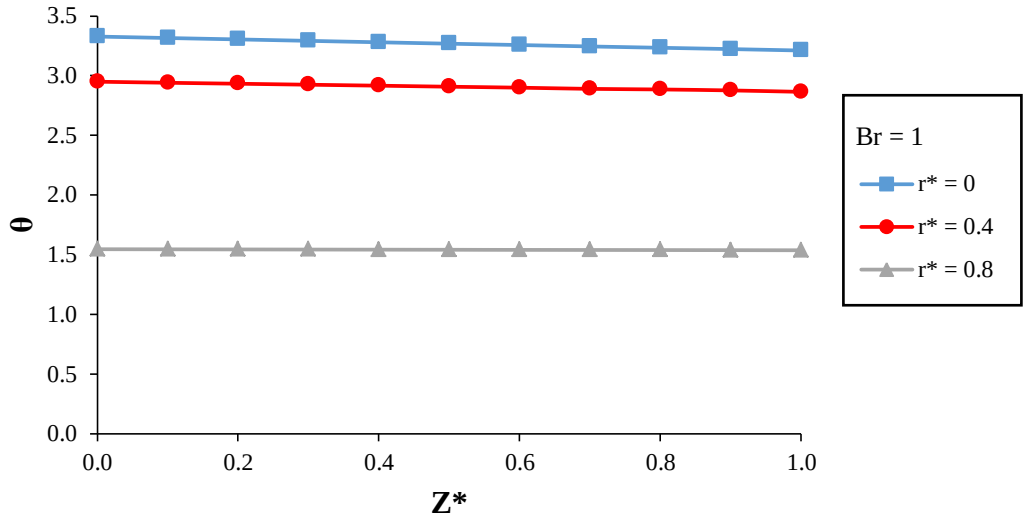

Figure 5: Laser rod temperature as a function of dimensionless length at different dimensionless radius for Br = 1

Figures 6-8 represent the variation of temperature with radial direction at different z* values for Br=0.001, 0.1 and 1, respectively. The figures illustrate that the temperature is maximum at the rod center and it decreases as the radial direction increases to approach the wall temperature at r*=1. The decrease in temperature with radial direction is steep for r* values larger than 0.4. Again, from the Br definition, the

temperature increases as Br increases for the same z* value. The results show that the temperature at z*=0 has the highest value for the same r* value whereas the temperature for all z* values approach the same value between r*= 0.6 and 1. The figures show that increasing Br number results in a decrease in the temperature difference which can be explained by the definition of Br number given in this work. Increasing Br number means higher heat generation within the laser rod.

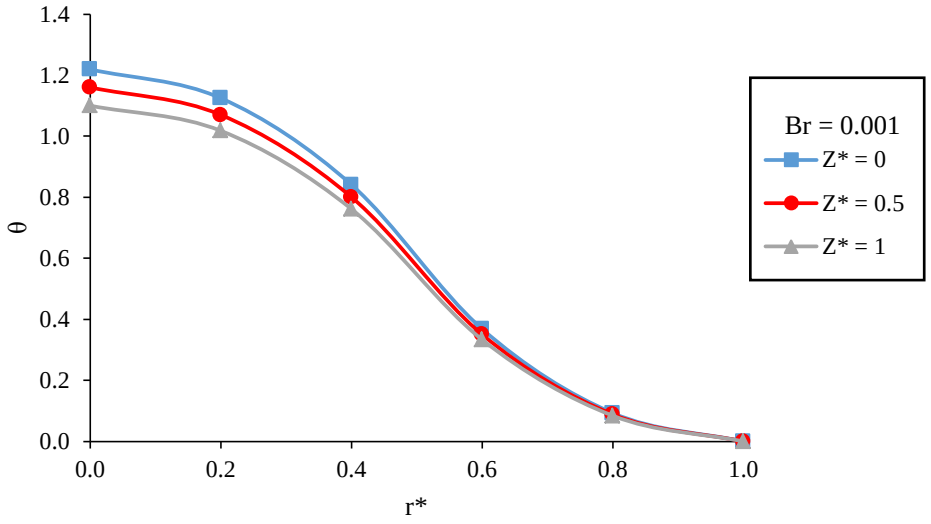

Figure 6: Laser rod temperature as a function of dimensionless radius at different dimensionless length for Br = 0.001

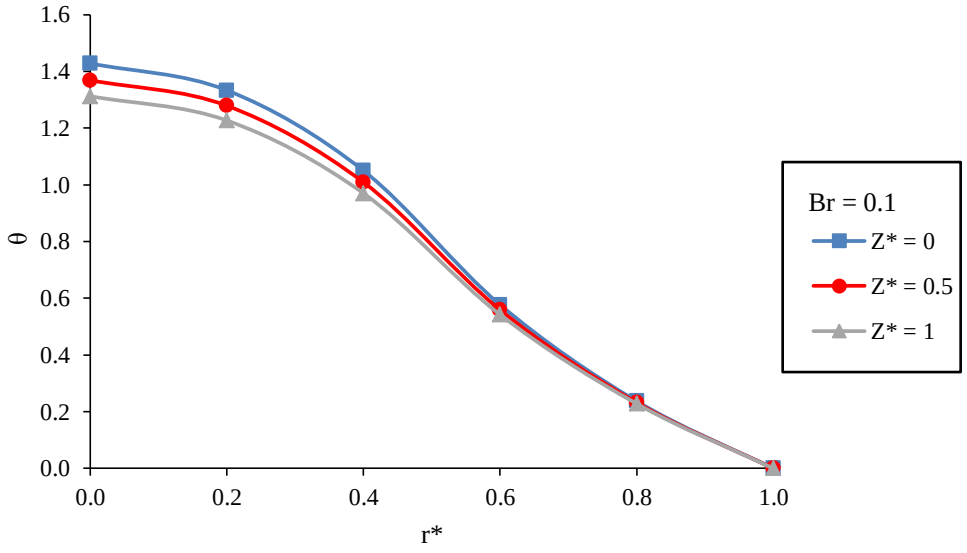

Figure 7: Laser rod temperature as a function of dimensionless radius at different dimensionless length for Br = 0.1

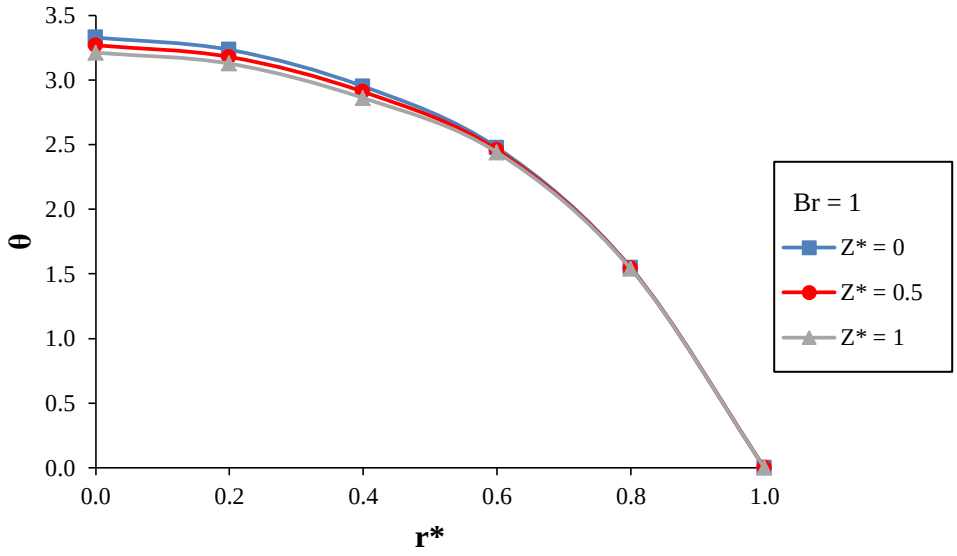

Figure 8: Laser rod temperature as a function of dimensionless radius at different dimensionless length for Br = 1

Figure 9 presents the effect of Br on the axial temperature distribution at the center of the laser rod. As can be seen from Figure 9, lower Br results in lower temperature. The difference in temperature distributions for low Br values (less than 0.1) is not high. Hence, high Br value keeps the rod temperature high. The temperature distribution is linear with all Br values in the radial direction. The radial temperature distribution with different Br values can be proved to exponentially decreasing with radial direction for Br = 1, however, this decrease is slower for Br = 0.001 and 0.1. Again, for these two Br values, the temperature distributions are close to each other whereas for Br =1 the temperature has large values.

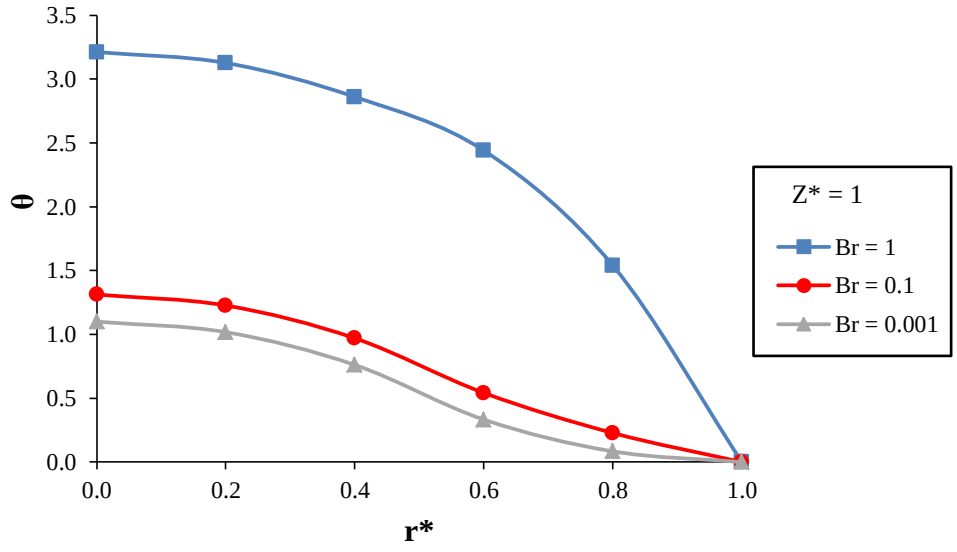

Figure 9: Laser rod temperature as a function of dimensionless radius at different Brinkman number

4. Conclusion

A complete analytical model was used to determine closed expressions for laser rod and fluid temperatures. The main idea behind this simplified work is the large aspect ratio considered in the analysis which resulted in obtaining the differential equations in r direction only. All the expressions are expressed in terms of Br number which in fact includes the term of the internal heat generation of the laser rod. But due to the fact that volumetric heat generation is function of radial and axial directions, the temperature distributions are function of both r and z. The results are plotted as function of Br number. The main output of this work that it is better for cooling purposes to have low Br values which can be achieved by having low internal heat generation of the laser rod.

Nomenclature

A_r aspect ratio

Br Brinkman number

c_p specific heat (J/kgK)

k thermal conductivity of fiber (W/mK)

L laser rod length(m)

Q absorbed power (W)

q_v volumetric heat generation (W/m^3)

P_o pumping power (W)

P_r Prandtl number

r radius (m)

T temperature (m)

u velocity (m/s)

z axial direction (m)

Greek letters

α absorption coefficient

ρ density (kg/m^3)

μ dynamic viscosity (kg/ms)

ξ thermal factor

Subscripts

f fluid

i internal

m mean

o outer

w wall

References

[1] Aldelaimi, A.A.K., T.N. Aldelaimi, and S.M. Al-Gburi, *Using of Diode Laser (940 nm) in Orofacial Region.* Journal of Research in Medical and Dental Science, 2017. **5**(5): p. 34.

[2] Rodrigues, G.C., C. Decroos, and J.R. Duflou, *Considerations on assist gas jet optimization in laser cutting with direct diode laser.* Procedia Engineering, 2017. **183**: p. 37-44.

[3] Rodrigues, G.C., et al., *Theoretical and experimental aspects of laser cutting with a direct diode laser.* Optics and Lasers in Engineering, 2014. **61**: p. 31-38.

[4] C. Rodrigues, G. and J.R. Duflou, *Into polarization control in laser cutting with direct diode lasers.* Journal of Laser Applications, 2016. **28**(2): p. 022207.

[5] Bachmann, F., P. Loosen, and R. Poprawe, *High power diode lasers: technology and applications*. Vol. 128. 2007: Springer.

[6] Knight P. L, M.A., *Diod Laser Arrays.* Cambridge University Press: p. 464.

[7] INTECH, *Heat Generation and Removal in Soild State Lasers.* accessed 15 March, 2018.

[8] He, G., et al., *Generation of radially polarized beams based on thermal analysis of a working cavity.* Optics express, 2011. **19**(19): p. 18302-18309.

[9] He, W.-J., et al., *Diode-pumped efficient Tm, Ho: GdVO 4 laser with near-diffraction limited beam quality.* Optics express, 2006. **14**(24): p. 11653-11659.

[10] Zhu, X. and N. Peyghambarian, *High-power ZBLAN glass fiber lasers: review and prospect.* Advances in OptoElectronics, 2010. **2010**.

[11] Jeong, Y.-C., et al., *Multi-kilowatt single-mode ytterbium-doped large-core fiber laser.* Journal of the Optical Society of Korea, 2009. **13**(4): p. 416-422.

[12] Ahmed, M.A., et al., *High-power radially polarized Yb: YAG thin-disk laser with high efficiency.* Optics express, 2011. **19**(6): p. 5093-5103.

[13] Beil, K., et al., *Thermal and laser properties of Yb: LuAG for kW thin disk lasers.* Optics express, 2010. **18**(20): p. 20712-20722.

[14] Dascalu, T. and T. Taira, *Highly efficient pumping configuration for microchip solid-state laser.* Optics express, 2006. **14**(2): p. 670-677.

[15] Bhandari, R. and T. Taira, *Megawatt level UV output from [110] Cr 4+: YAG passively Q-switched microchip laser.* Optics express, 2011. **19**(23): p. 22510-22514.

[16] Innocenzi, M., et al., *Thermal modeling of continuous-wave end-pumped solid-state lasers.* Applied Physics Letters, 1990. **56**(19): p. 1831-1833.

[17] Brown, D.C. and H.J. Hoffman, *Thermal, stress, and thermo-optic effects in high average power double-clad silica fiber lasers.* IEEE Journal of quantum electronics, 2001. **37**(2): p. 207-217.

[18] Shi, P., et al., *Semianalytical thermal analysis of the heat capacity of YAG laser rods.* Applied optics, 2009. **48**(35): p. 6701-6707.

[19] Shi, P., et al., *Semianalytical thermal analysis on a Nd: YVO 4 crystal.* Applied optics, 2007. **46**(19): p. 4046-4051.

[20] Shi, P., et al., *Semianalytical thermal analysis of thermal focal length on Nd: YAG rods.* Applied optics, 2007. **46**(26): p. 6655-6661.

[21] Zhu, X. and R. Jain, *10-W-level diode-pumped compact 2.78 μm ZBLAN fiber laser.* Optics letters, 2007. **32**(1): p. 26-28.
[22] Tokita, S., et al., *Liquid-cooled 24 W mid-infrared Er: ZBLAN fiber laser.* Optics letters, 2009. **34**(20): p. 3062-3064.
[23] Sangla, D., et al., *High power laser operation with crystal fibers.* Applied Physics B, 2009. **97**(2): p. 263.
[24] Liu, T., Z. Yang, and S. Xu, *3-Dimensional heat analysis in short-length Er 3+/Yb 3+ co-doped phosphate fiber laser with upconversion.* Optics express, 2009. **17**(1): p. 235-247.
[25] Pfistner, C., et al., *Thermal beam distortions in end-pumped Nd: YAG, Nd: GSGG, and Nd: YLF rods.* IEEE Journal of Quantum Electronics, 1994. **30**(7): p. 1605-1615.
[26] Li, L., et al., *3-Dimensional thermal analysis and active cooling of short-length high-power fiber lasers.* Optics express, 2005. **13**(9): p. 3420-3428.
[27] Ashoori, V. and A. Malakzadeh, *Explicit exact three-dimensional analytical temperature distribution in passively and actively cooled high-power fibre lasers.* Journal of Physics D: Applied Physics, 2011. **44**(35): p. 355103.
[28] Shibib, K.S., M.A. Minshid, and N.E. Alattar, *Thermal and stress analysis in nd: yag laser rod with different double end pumping methods.* Thermal Science, 2011. **15**, supp. 2: p. S399-S407.
[29] Shibib, K.S., M.M. Taher, and M.A. Mahdi, *Analytical treatment of transient temperature and thermal stress distribution in cw-end-pumped laser rod: Thermal Response Optimization Study.* Thermal science, 2014. **18**(2): p. 399-408.
[30] Shibib, K.S., et al., *Transient analytical solution of temperature distribution and fracture limits in pulsed solid state laser rod.* Thermal Science, 2017. **21**(3): p. 1213-1222.
[31] Assad, M.E.H. and D.C. Brown, *Thermodynamic analysis of end-pumped fiber lasers subjected to surface cooling.* IEEE Journal of quantum electronics, 2013. **49**(1): p. 100-107.
[32] Jiang, H.J., et al., Three-dimensional transient thermodynamic analysis of laser surface treatment for a fiber laminated plate with a coating layer. International Journal of Heat and Mass Transfer, 2018. **118**: p.671-685.
[33] Jiang, H.J., et al., An analytical solution of three-dimensional steady thermodynamic analysis for a piezoelectric laminated plate using refined plate theory. Composite Structures, 2017, **162**: p. 194-209.
[34] Jiang, H.J., et al., Three-dimensional steady thermodynamic analysis for a double-layer plate with a local heat source and harmonic load. Applied Thermal Engineering, 2016, **106**: p. 161-173.
[35] Assad, M.E.H., *Effect of maximum and minimum heat capacity rate on entropy generation in a heat exchanger.* International Journal of Energy Research, 2010. **34**(14): p. 1302-1308.
[36] Assad, M.E.H., *Entropy generation analysis in a slab with non-uniform heat generation subjected to convection cooling.* International Journal of Exergy, 2011. **9**(3): p. 355-369.
[37] Assad, M.E.H., Study of entropy generation in a slab with non-uniform internal heat generation. Thermal Science, 2013,**17**(3): p. 943-950.